Physics of Plasmas

Positive charging of grains in an afterglow plasma is enhanced by ions drifting in an electric field

Cite as: Phys. Plasmas **28**, 103702 (2021); https://doi.org/10.1063/5.0069141
Submitted: 29 August 2021 • Accepted: 24 September 2021 • Published Online: 13 October 2021

Neeraj Chaubey, J. Goree, Steven J. Lanham, et al.

Physics of Plasmas ARTICLE scitation.org/journal/php

Positive charging of grains in an afterglow plasma is enhanced by ions drifting in an electric field

Cite as: Phys. Plasmas **28**, 103702 (2021); doi: 10.1063/5.0069141
Submitted: 29 August 2021 · Accepted: 24 September 2021 ·
Published Online: 13 October 2021

View Online Export Citation CrossMark

Neeraj Chaubey,[1,a)] J. Goree,[1] Steven J. Lanham,[2] and Mark J. Kushner[2]

AFFILIATIONS

[1]Department of Physics and Astronomy, University of Iowa, Iowa City, Iowa 52242, USA
[2]Department of Electrical Engineering and Computer Science, University of Michigan, 1301 Beal Avenue, Ann Arbor, Michigan 48109-2122, USA

[a)]Author to whom correspondence should be addressed: neeraj-chaubey@uiowa.edu

ABSTRACT

In a plasma, the polarity of a dust grain's charge is typically negative, but it can reverse and become positive in an afterglow, when the power sustaining the plasma is switched off. This positive charging, which occurs in the afterglow's first few milliseconds, is studied for grains much larger than a few nm. It is hypothesized that the positive charging is enhanced by the presence of a dc electric field, which causes ions to drift through the neutral gas. A larger value of the reduced electric field E/N leads to a larger ion kinetic energy and thus a greater collection of positive charge on a grain. The maximum possible positive charge is attained if the grain's surface potential rises to match the ion kinetic energy, at a time before ions have departed and the grain's charge becomes frozen. Thereafter, when vacuum conditions prevail, the grain will retain its positive residual charge. In an experiment, dust grains were electrically levitated in a capacitively coupled plasma until the power was abruptly turned off. In the afterglow, grains fell faster than expected due to gravity alone, indicating a downward electric force, in the presence of a remaining dc electric field. Acceleration measurements yielded repeatable results for the residual charge's value, which was of the order $+10^4$ e and increased with E/N, supporting the hypothesis.

I. INTRODUCTION

Dust grains in a plasma gain an electric charge by collecting electrons and ions. The charge on the grain develops so that there is a balance in the collection of electrons and ions, under steady conditions.[1–9] The grain's surface potential, which is also called the floating potential, is proportional to this charge.

The polarity of the charge depends on the type of plasma. A positive charge can occur in space plasmas, due to photoemission in the presence of ultraviolet sunlight.[10–12] Similarly, positive charges may occur due to thermionic or secondary emission of electrons,[9,10] for example, in fusion plasmas.[13] However, a negative charge is most common in low-temperature laboratory plasmas. In particular, in a laboratory glow-discharge plasma, a micrometer-size grain generally attains a substantial negative charge equivalent to thousands of electronic charges.[14–24] This large negative charge is well known to occur under steady conditions, but for unsteady conditions, the charge can be different.

An unsteady condition that has gained recent interest, for dust grain charging, is a temporal afterglow.[25–41] Such an afterglow occurs after extinguishing the source of power that sustains the ionization in a glow-discharge plasma. (For this discussion, in the absence of dust grains, we assume a plasma consisting of only electrons and positive ions.) The first development, within tens of microseconds, is a rapid cooling of energetic electrons.[25–29] Then, over a longer time period of a few milliseconds there is a gradual loss of plasma density. This density loss of electrons and ions might initially be balanced, but only up to a point.[25–29] When the plasma density falls below the ambipolar limit, the fluxes of electron and ions are no longer constrained to be the same. At this point, the transition to free diffusion, the electron flux out of the plasma exceeds that of positive ions. The more rapid loss of electrons leads to a comparatively greater abundance of ions, a condition that has sometimes been called "uncompensated ions."[32] It is this condition, in which there are uncompensated ions, that offers the possibility that a grain's charge can reverse polarity, and become positive. Ultimately, when both electrons and ions have departed, the grain is left with a long-lasting residual charge.[26,27,29,32]

In addition to temporal afterglows, another kind of afterglow is a spatial afterglow.[42–48] The experimental configuration is typically a glass tube, with a gas inlet at one end, plasma generation by radio

frequency (rf) power in the middle, and an exhaust at the other end. This setup has a practical use as a reactor for synthesizing nanoparticles with unusual properties.[49–51] In a spatial afterglow, which is generally steady in time, the plasma density is less than in the main plasma where ionization takes place. Depending on the configuration of the apparatus, for example, when grids are used to collect electrons, it is possible for a spatial afterglow to have an unbalanced loss of electrons and ions, so that there are uncompensated ions.[43,47,48]

A grain's charge becomes less negative when a plasma enters the condition of either a temporal[25] or spatial[43] afterglow. This diminishment of negative charge has been described as "decharging."[25]

More interesting than just a diminishment of a negative charge, however, is a polarity reversal. Such a reversal has been reported in several experiments in which positive charges on grains in an afterglow plasma were detected.[32,43,47] A positive charge is noteworthy because negative charging of dust grains is typically the rule in laboratory plasmas. We should mention, however, that these experiments have until now been in an early point of development, so that their results for charging sometimes included unexplained effects. In particular, there were often large variations in the charge from one observation to the next. We review these afterglow experiments, with observations of positive charging, in Sec. II.

In this paper, we develop a model to explain positive charging of dust grains in the afterglow of low-pressure plasmas. We present this model as a hypothesis, in Sec. III. It is based on theoretical models developed by other authors,[25–27,29,32] but with an added emphasis on the role of a dc electric field. In our hypothesis, the electric field, in combination with gas friction, determines the kinetic energy of ions as they drift through the gas, in an afterglow. This ion kinetic energy is crucial for charging as it determines the maximum positive charge that can be attained, for a grain in an afterglow.

We also report an experiment in which we detect large positive charges. As in previous experiments[25,32,43,47] ours had a dc electric field during the temporal afterglow, but otherwise our experiment was configured differently. We suddenly turned off the rf power that sustained the plasma, and observed the grains with a video camera, as they fell. Measuring their acceleration, and subtracting the effect of gravity, allowed us to determine the electric force, as in Ref. 52. Dividing that electric force by the dc electric field yielded the charge. The charge we measured was always positive, and it was consistent from one observation to the next. The magnitude of the positive charge was of the order $+10^4$ e, which is much larger than in most previous experiments. Our experiment is described in Sec. IV.

An analysis of our experimental results in Sec. V leads to a test of our hypothesis in Sec. VI. The outcome of this test is a good agreement in explaining the positive charging. The measurement closely matches the prediction for the maximum positive charge.

Dust grains can be used as a probe to measure conditions within a plasma sheath, as reported by previous authors,[53–59] who used steady plasma conditions. Our result suggests that grains can also be used to probe in an afterglow plasma, as we explain in Sec. VII.

We present our summary in Sec. VIII.

II. PREVIOUS AFTERGLOW EXPERIMENTS WITH POSITIVE CHARGE

Here, we review three previous experiments in which a positive charge was detected for grains in an afterglow plasma.[32,43,47,60] In all three of these experiments, there were two significant features: a dc electric field applied during the afterglow, and video imaging to analyze the grain's motion in response to the dc electric field.

In 2013, Wörner *et al.*[32] reported on an experiment where 6.8 μm microspheres in a temporal afterglow were observed with a positive charge as large as $+50$ e. Their experiment was performed under microgravity conditions, orbiting the Earth on the International Space Station, so that acceleration by gravity was not a factor. Grains were introduced into a plasma sustained in argon (pressure 20 Pa) that was generated by rf power applied to parallel-plate electrodes. Then, the rf power was turned off, resulting in an afterglow. During the afterglow, a dc electric field of 6.67 V/cm was purposefully applied in the direction perpendicular to the two parallel-plate electrodes. Grains in the inter-electrode region were observed by video cameras. Due to the lack of gravitational acceleration, the experimenters were able to observe their grains for an extended time in the afterglow. The authors mentioned that ions remained in the afterglow longer than electrons, in the inter-electrode region.

In 2020, Minderhout *et al.*[43] reported on a spatial afterglow experiment, with 4.9 μm microspheres that developed positive charges as large as $+10$ e. This experiment was performed in the laboratory, in a vertically oriented glass tube. Grains were introduced into the top of the tube, and they fell downward. The main plasma, sustained in argon (90 Pa), was operated continuously in an upper volume of the tube, which was separated from a downstream volume by a grounded mesh grid. Within the downstream volume, which was described as a "shielded spatial afterglow," both electrons and ions were present, but had a lower density than in the main plasma. Within this downstream or afterglow volume there were grains, which were observed moving horizontally in response to a purposefully applied horizontal dc electric field. The field was adjustable up to 50 V/cm, resulting in a measurable deflection of grain trajectories, so that their charges could be determined. (The authors also noted that, aside from allowing this measurement of the charge, the dc electric field also augmented the plasma density in the spatial afterglow.) This experiment was complicated by a wide dispersion of results for the charges for individual grains. Similar results were obtained in a follow-up experiment[47] in which the plasma power was pulsed rather than continuous.

Later in 2020, Schneider's Ph.D. thesis[60] thesis reported on an experiment with a temporal afterglow with a positive charge much larger than in the earlier experiments. The dc electric field applied during the afterglow was of the order 10^2 V/cm. Based on video observations of the motion of a single microsphere, Schneider reported charge measurements, which had a dispersion varying from negative to positive for different observations. The maximum positive charge detected was $+5000$ e. In further tests, Schneider found that the grain's charge in the afterglow did not depend significantly on the rf power, gas pressure, or the grain's position above the electrode.

The authors of the three recent papers mentioned above[32,43,60] all used the term "afterglow" to describe the environment that was experienced by their grains that developed positive charges. We should also mention an earlier experiment, reported in 2007 by Wang *et al.*,[20] in which positive charges greater than $+500\,000$ e were detected on their large ($\geq$100 μm) grains. Although Wang *et al.* did not use the term "afterglow" to describe their experiment, some of their runs have some similarities to the experiment of Minderhout *et al.*[43] In both experiments, plasma was generated constantly in an upper volume, while in

a lower volume there was a detection of grain charges. Instead of a mesh to separate the two volumes, Wang *et al.* used a plate with a small hole. Their plate, like the mesh of Minderhout *et al.*, had a bias for repelling electrons, so that grains in the plate's vicinity, and below it, were exposed to ion-rich conditions. Thus, we suggest that the early experiment of Wang *et al.* should perhaps be included in the discussion of positive grain charging in a spatial afterglow.

III. MODEL OF CHARGING IN THE AFTERGLOW

A. Previous models

Charging models for dusty plasmas have long recognized that a grain in a plasma has a charge that is not fixed, but varies with time as

$$dQ_d/dt = J_i - J_e, \tag{1}$$

where J_i and J_e are the ion and electron currents collected on the grain.[61] (This discussion assumes that other contributions to charging, such as photo- or thermionic emission of electrons, are not important.) These currents are proportional to the ion and electron densities, respectively, and depend also on the characteristic velocities of the ions and electrons. If the conditions for the electrons and ions are steady, so that the left-hand side of Eq. (1) is zero, there will be an equilibrium charge that is seldom zero, if the grain is larger than a few nm. Its polarity will be generally negative, due to the smaller velocities of ions as compared to electrons (assuming that the plasma is quasineutral).[10]

However, if the electron and ion conditions are not steady, but change with time, the grains will have a characteristic charging time.[10] A key point is that this charging time will be inversely proportional to the plasma density n. In a plasma that is neutral (i.e., $n_e = n_i$), with electrons and ions that have thermal distributions of velocity, the charging time can be expressed as in Ref. 62,

$$\tau = K_\tau \frac{(k_B T_e)^{1/2}}{Rn}, \tag{2}$$

where R is the radius of a spherical grain, T_e is the electron temperature, and the constant K_τ is of the order 10^3 s μm cm^{-3} eV$^{-1/2}$, with a precise value[62] that depends on the values of T_i/T_e and m_i/m_e. In Eq. (2), we see the inverse scaling of charging time with plasma density n, which is particularly important in the development of afterglow plasmas: as the density declines, the charging time becomes longer.

The unsteady conditions that are of interest in this paper are those of a temporal afterglow plasma. For this situation, Ivlev *et al.*[25] described how a grain's charge changes from its equilibrium value, after extinguishing the power that sustained the plasma. The development of the charge occurs not all at once, but in a sequence of stages, as described by Couëdel *et al.*[26,27,29] and Wörner *et al.*[32] As numbered by Couëdel *et al.*, these are stages 1–4, which we summarize next.

Stage 1 begins when the power that sustained the plasma is switched off. During this stage, the electron temperature diminishes rapidly as the electrons are cooled by inelastic and elastic collisions with room-temperature neutral atoms. Thus, the current J_e diminishes more rapidly than the current J_i, in Eq. (1). This initial stage can be the quickest of all, depending on the density of neutral atoms. During this rapid diminishment, the charge remains negative.

Stage 2 begins after the rapid cooling of electrons has abated. In the main plasma region, the electrons and ions remain quasineutral, and they undergo ambipolar transport toward the boundaries of the plasma chamber. Ambipolar transport constrains the flux of electrons and ions leaving the plasma to be equal by generating electric fields that slow down the more mobile electrons and speed the less mobile ions. As this transport proceeds, there is a continuous loss of electrons and ions from the main plasma region, so that their densities are in constant decline.

Stage 2 ends when the transport of ions and electrons changes due to a reduced density. One mechanism for this change is the reduction of electric fields within the boundary sheaths, as they thicken. At that point, the fields can no longer slow the ions and sustain ambipolar transport, and thereafter electrons can be lost from the chamber volume more rapidly than ions. (Couëdel *et al.*[26,27,29] also proposed an additional mechanism for a change in the plasma transport, centering on the depletion of electrons by collecting on dust grains rather than the chamber walls; this can be significant in some experiments, but not in ours.)

Stage 3 is of great interest because it is during this time interval that the grain's charge can trend toward a positive value. This trend occurs due to a greater abundance of ions as compared to electrons, a situation termed "uncompensated ions" by Wörner *et al.*[32] This mismatch of ion and electron densities arises from the greater loss of electrons to surfaces, after the end of quasineutral transport. During stage 3, due to their smaller mass the electrons are lost from the chamber volume much faster than ions. Thus, in stage 3 there will be uncompensated ions, so a grain will collect more ions than electrons. Under these conditions, the right-hand side of Eq. (1) will be positive, and the grain's charge will trend to a less negative value.

Importantly, beyond just trending to a less negative charge, the grain can continue charging positively long enough to actually reverse sign, and gain a positive value. This charge reversal requires sufficient time and sufficient ion current to the grain.[32]

In the final stage 4, the density of uncompensated ions diminishes to the point where the ion current becomes insufficient to further change the grain's charge significantly, no matter how much time passes. The charge then becomes "frozen," as described by Ivlev *et al.*[25]

Whether the grain attains its maximum possible residual charge depends on the timing of the onset of the frozen condition. If the charging time is too long, the charge will become prematurely frozen, and fall short of its maximum possible value. Perhaps due to this charging-time issue, Couëdel *et al.*[26,27] found that their model is unable to predict a positive charge, even though they observed positive charges in their experiment. For our experiment, we believe that this premature freezing did not occur, as we will explain later.

B. Model with mobility-limited ion motion

Here, we develop a model to predict the maximum possible residual charge of a grain, $Q_{\rm res}^{\rm max}$ after electrons and ions have departed the plasma volume. As compared to the previous models described above, the key difference is that we account for ions that move not with a slow random thermal velocity, but a faster drift velocity due to a dc electric field. This approach yields a quantitative prediction for $Q_{\rm res}^{\rm max}$ as well as for a corresponding maximum surface potential for the grain.

In an afterglow plasma, under conditions where electrons are nearly absent, two factors that play a great role in determining the positive charge of a grain are the ion kinetic energy and the time available

for a grain's charge to change. If there is sufficient time for the grain to attain its maximum possible positive charge, the value of that charge will be determined by the ion kinetic energy. A larger energy will allow a larger maximum possible positive charge.

For the ion kinetic energy, we will not assume that we have a non-drifting thermal distribution of velocities. Such an assumption was made by previous investigators, and for that reason their models predicted a rather modest value for the maximum possible residual charge, for example, $\approx +100$ e, for a grain with a radius of a few micrometers.[32]

As an advance on the models of the previous investigators, we note that the ion kinetic energy is enhanced in the presence of an electric field. (Such an electric field might be added purposefully as in Refs. 32 and 43 or it might occur naturally, as in our experiment, from the persistent negative dc bias on a powered electrode.) This enhancement of the ion kinetic energy will be modeled by assuming mobility-limited ion motion, which involves a balance of two forces governing the ion energy. The Coulomb force q_{iE} accelerates ions of charge q_i, while a frictional force on the neutral gas slows them. The latter force is proportional to the neutral gas density N. When these two forces are balanced, ions drift at a constant velocity,

$$\nu_i = \mu_i E, \tag{3}$$

where μ_i is the ion mobility coefficient. This mobility-limited ion velocity is applicable when the mean-free-path for ion-neutral collisions is much shorter than the scale length for the electric potential variation. (Of course, the ions will not be exactly monoenergetic, but will have a velocity distribution,[63] with some moving a little slower or faster.)

In general,[64] the mobility μ_i depends on the reduced electric field E/N. The traditional unit for E/N is the Townsend, where $1\,\mathrm{Td} = 10^{-17}\,\mathrm{V\,cm^2}$. For afterglow experiments with dust grains, typical values of E/N are of the order 10^2 Td if the gas pressure is hundreds of mTorr as in previous afterglow experiments,[32,43] or in the range 10^3–10^4 Td as in our experiment, which had a much lower gas pressure.

Making use of Frost's semi-empirical expression for mobility, we can rewrite Eq. (3) as in Refs. 65 and 66,

$$\nu_i = \alpha \frac{E}{N}\left[1 + \beta \frac{E}{N}\right]^{-1/2}, \tag{4}$$

so that the mobility can be written as

$$\mu_i = \alpha \frac{1}{N}\left[1 + \beta \frac{E}{N}\right]^{-1/2}. \tag{5}$$

These expressions are intended to obey a physically meaningful power-law scaling, in their asymptotic limits. The mobility in Eq. (5) is either constant or $\propto (E/N)^{-1/2}$, at low and high E/N, respectively. These two limits correspond to two regimes: weak field or strong field, for ions drifting much slower or faster than the thermal speed, respectively.

The coefficients α and β depend on the atomic species, and α also depends on the gas temperature. These coefficients are empirically obtained by fitting Eq. (4) to archival experimental data for ν_i vs E/N. For Ar^+ in Argon gas, using data[67] from drift-tube experiments at 300 K, our fit results are $\alpha = 4.95$ (m/s Td) and $\beta = 0.0098$ (1/Td).

The maximum possible surface potential for a grain is determined by the kinetic energy of the ions. The key concept is that ions are collected until the grain's potential becomes so positive that it repels the ions.

In the presence of mobility-limited ion motion, this condition occurs at a maximum surface potential,

$$V_{\mathrm{float}}^{\mathrm{max}} = K_i/e = \frac{1}{2e} m_i \mu_i{}^2 E^2. \tag{6}$$

Likewise, the maximum possible residual charge is

$$Q_{\mathrm{res}}^{\mathrm{max}} = \frac{2\pi\epsilon_0 R m_i \mu_i^2 E^2}{e}. \tag{7}$$

To obtain Eq. (7), we have used the standard expressions[7] for dust-grain charging, modeling the dust grain as a spherical capacitor, $Q_{\mathrm{res}} = CV_{\mathrm{float}}$ and $C = 4\pi\epsilon_0 R$.

These expressions assume that the grain radius R is much less than the screening length, as is the case of our experiment. For a dielectric grain, these expressions assume uniform charging of the grain's surface, so that the fields surrounding the grain mimic those due to a conducting sphere; we neglect any asymmetric charging.

C. Hypothesis

We can formulate the model presented above as a hypothesis, so that we can test it experimentally. Our hypothesis is that the maximum possible values of the positive potential and charge, for a grain in an afterglow, are determined by E/N. The ion kinetic energy will be enhanced above thermal levels, if there is a finite value of E/N. This enhanced ion energy will promote a greater positive charging of a grain. In the situation where the mobility-limited velocity of ions greatly exceeds their thermal velocity, we can predict the value of the maximum positive potential and charge using Eqs. (6) and (7), in combination with Eq. (5) for the ion mobility. After we test this hypothesis experimentally in Sec. VI, and find agreement, we can reliably use it as a model.

D. Simplifying assumption

In using the model, the electric field is an important input for Eqs. (6) and (7) to obtain the floating potential and residual charge. If the electric field varies in time, it would be appropriate to evaluate the field at the moment when the charge becomes frozen. In general, obtaining the electric field at that moment would require a time-dependent modeling of both charging and electric field. The charging would be modeled using Eq. (1), while the electric field would be modeled using Poisson's equation. The right-hand side of both of these equations depend on the ion density, which in turn depends on time.

Performing this modeling in detail would not be a trivial effort. Indeed, it would be impractical if the user lacks detailed time-series data for ion density, which is the situation we will face, in testing our hypothesis.

Not having a time series of ion-density data, a simplifying assumption must be made, centering on the relative timing of two events: when the grain's charge becomes frozen, and when the electric field has nearly attained its vacuum condition.

Our assumption is that the grain's charge becomes frozen at a time after the electric field has nearly attained its vacuum condition.

In other words, the charging equation relaxes to its asymptotic solution after Poisson's equation does so. Equivalently, the assumption is that ions, as they gradually diminish in density, will continue to have an effect in charging the grains at a time when they no longer have a significant effect on the electric field.

IV. EXPERIMENT

A. Apparatus

The experiment was performed using our Kuda-Topf plasma chamber.[68,69] The vacuum chamber, which is made of stainless steel, has an interior that is mostly cylindrical. A horizontal lower electrode was powered, while the chamber itself was grounded. The dimensions are shown in Fig. 1; a photograph and mechanical drawing are provided in the supplementary material.

A low gas pressure was used, allowing us to easily achieve a large value of E/N. We thereby attained a high-velocity drift of ions in the afterglow. The argon gas pressure was 8.00 mTorr (1.067 Pa), which was monitored by a capacitance manometer, and regulated by a feedback controller. The gas was in good thermal contact with the vacuum chamber, at room temperature, which we measured as $T = 295\,^{\circ}\mathrm{K}$. (This value was close to the 300 °K argon temperature for the drift tube mobility data,[67] so that we use those data without correcting for temperature.) The gas number density was $N = P/k_B T = 2.82 \times 10^{20}\ \mathrm{m}^{-3}$.

During steady plasma operation, we sustained the plasma with a radio frequency voltage applied to the lower electrode. As shown in Fig. 1, a waveform at 13 MHz was produced by an Agilent 33220A function generator, which was connected to an Amplifier Research 150A100B Class A amplifier and an impedance matchbox. The apparatus was operated in a capacitively coupled plasma (CCP) configuration by including a coupling capacitor C_{coupl}, between the matchbox and the powered lower electrode.

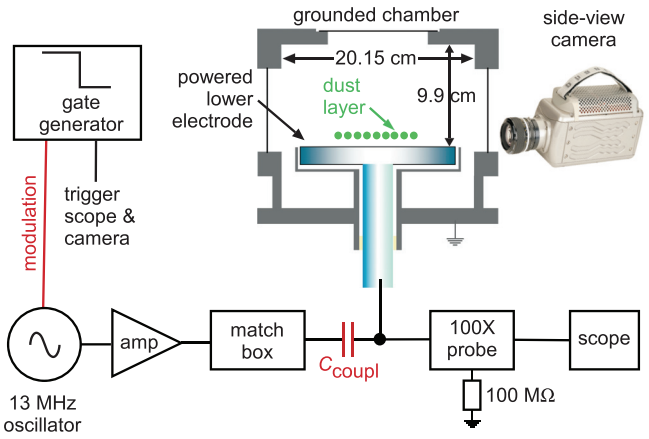

FIG. 1. Experimental setup. During plasma operation, the modulation signal was on, allowing rf power to be applied to the lower electrode, and a plasma was formed. Because of capacitor C_{coupl}, the lower electrode developed a negative dc self-bias. This self-bias helped electrically levitate grains in a 2D layer during plasma operation. When the modulation signal was switched off, the rf power extinguished, and at that moment an oscilloscope was triggered, and a side-view video camera began recording. Grains were illuminated by a vertical sheet of laser light, not shown here. During the afterglow, the lower electrode retained most of its negative dc bias due to the capacitor C_{coupl}. The bias on the lower electrode was measured using a Tektronix 100X probe. Its 100 MΩ impedance, in combination with C_{coupl}, provided a long discharge time constant of 3 s, so that a negative electrode bias remained throughout the afterglow.

The plasma filled a cylindrical space above the lower electrode. We will refer to this space as the plasma volume, which was 3.1 l. The spatial distribution of the electron density and electron temperature within the chamber were modeled, during steady plasma operation, yielding profiles presented in the supplementary material. The model used was the hybrid plasma equipment model (HPEM) code at the University of Michigan.[77]

The capacitor C_{coupl} played a significant role in our experiment. During plasma operation, this 50 nF capacitor coupled the rf power to the lower electrode, as shown in Fig. 1, allowing a negative dc bias to be maintained on the lower electrode. This dc bias is a natural outcome of balancing currents in rf plasmas. We measured the dc self-bias, denoted $V_{electrode}$, using a digital oscilloscope with a 100× probe located on the atmospheric side of the electrode feedthrough.

During the afterglow, the capacitor gradually discharged, but due to its large capacitance, it did not discharge greatly during the time range of interest in this paper. As shown in the supplementary material, the capacitor discharged in two stages: rapidly at first due to collecting ions, over a timescale of a few milliseconds, and then a much slower exponential e-folding time that we measured as about 3 s. The latter value is the product of C_{coupl} with a 60 MΩ resistance, which is presumably due to the probe impedance of 100 MΩ in parallel with stray resistances.

The dust grains were polymer microspheres made of melamine-formaldehyde. The grains were exposed to vacuum for several months before the experiment began. At the beginning of each experimental run, we introduced approximately 2000 grains into the plasma from above, by agitating a dispenser that had a single small opening.

The mass of the grains will be important later, in obtaining the value of the grain's charge in the afterglow. Ours had a mass $m_d = 5.2 \times 10^{-13}$ kg, based on the manufacturer's specifications[80] for a diameter of 8.69 μm and a mass density of 1.51 g/cm^3.

During the plasma operation, the steady levitation of the grains was aided by the negative dc self-bias $V_{electrode}$ of the lower electrode. This levitation indicates that the grains had a negative charge. A negative grain polarity is certainly the most common situation, in a plasma that is quasineutral, due to the higher thermal velocity of the less massive electrons. This negative charge must have been at least several thousand elementary charges, to levitate the grains. In fact, a value of −14 000 e was measured by Kananovich and Goree, using a phonon-spectrum method, in an experiment with the same chamber and same microspheres as ours.[69] (Compared to their measurement, our charge might differ only slightly, due to somewhat different plasma conditions, with an argon pressure of 13.5 mTorr instead of our 8.00 mTorr.)

To initiate a temporal afterglow, we switched off the rf power once for each experimental run. This switching of the rf power was done using the gating feature of the rf function generator. The modulation signal that we used as a gate was a square waveform, as sketched in Fig. 1. The 13 MHz rf waveform was maintained steadily, to power the plasma, until the modulation signal transitioned abruptly to the off condition, extinguishing the rf power. Simultaneously, data recording was started by triggering the side-view camera and the oscilloscope.

We imaged the dust using a pair of Vision Research Phantom v5.2 cameras, one viewing from the side and the other from the top.

The side-view camera provided most of our data, to observe the grains as they fell when we turned off the rf power. For that camera, we illuminated grains with a vertical sheet of light from a 671-nm diode laser. This vertical sheet had a horizontal thickness of 1 mm. The side-view camera was fitted with a 52-mm-focal-length Nikon macro lens, with a 10-nm bandpass filter to block light at wavelengths other than that of its illuminating laser. This side-view camera was operated at 600 frames/s, which we chose to provide adequate temporal resolution during the falling of the grains, without sacrificing the image brightness. The spatial resolution for this side-view imaging was 26.8 pixel/mm.

As a diagnostic to characterize conditions in the afterglow, we used a photomultiplier tube (PMT). The PMT was positioned with its photocathode near a window of the chamber, as shown in the supplementary material, so that no lens was required to collect light. We also used no filter or spectrometer, so that the PMT responded to the entire visible spectrum of light emitted by the gas, as it glowed in the chamber.

B. Experimental runs

We performed ten experimental runs. All were done with the same gas pressure of 8.00 mTorr, but with different values of the rf voltage applied to the lower electrode. Runs with a larger rf voltage also had a larger dc self-bias on the lower electrode, while the plasma was on. These conditions are tabulated in the supplementary material.

At the beginning of each run, after igniting the plasma, we agitated a dust dispenser at the top of the chamber. As dust grains fell from the dispenser, they became charged negatively and were electrically levitated. The dispenser was then withdrawn, to a location near the chamber wall, so that it would not disturb the plasma. At the end of each run, the rf power was extinguished using the gate generator, so that the grains fell to the lower electrode, where they remained.

C. Afterglow condition measurements

1. Electrode bias measurement

The voltage waveform $V_{\text{electrode}}(t)$ on the lower electrode offers indications of the electron and ion conditions, which developed in three distinct time intervals. This waveform is shown in Fig. 2.

For $t < 0$, when the rf power was on, the electrode had a large peak-to-peak voltage waveform that was centered at a negative value, which was the dc self-bias. This self-bias produced a dc vertical electric field, which was superimposed on the 13 MHz rf field. This dc electric field applied a substantial steady force to the ions toward the lower electrode.

For $0 < t < 2$ ms, after turning off the rf power, the electrode's negative bias $V_{\text{electrode}}(t)$ began to change. This change, while remaining small due to the large capacitor C_{coupl}, is nevertheless useful for offering insight into the electron and ion conditions. The bias waveform during the first 2 ms was non-exponential. The overall decrease in the electrode voltage during this initial interval, which we denote as $\Delta V_{\text{electrode}}$, was a few tens of volts, as tabulated in the supplementary material. We attribute this decrease in the electrode bias to the collection of positive charges, as ions reached the lower electrode.[70] This collection of ions occurred over a finite time interval, as ions flowed through the chamber to the lower electrode. This time interval of about 2 ms is our indication of the duration that ions were detectable in the afterglow; precise values are tabulated in the supplementary material.

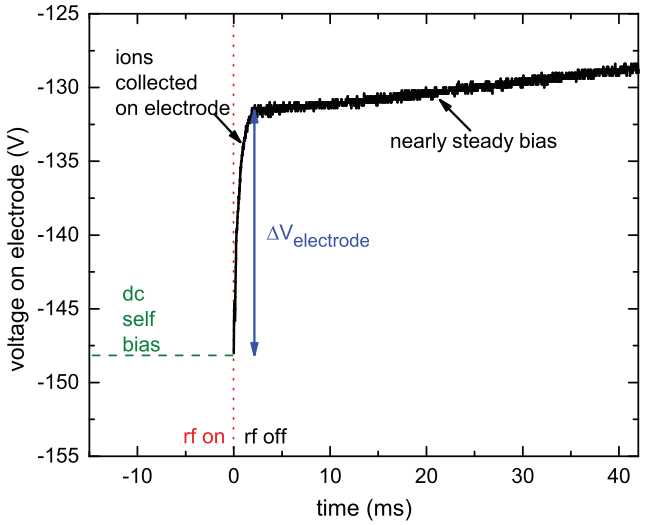

FIG. 2. Waveform for the bias $V_{\text{electrode}}$ on the lower electrode. The rf power was turned off at time $t = 0$. For $t < 0$, when the plasma was on, there was a dc self-bias, indicated here, as well as a large-amplitude oscillatory waveform that is not shown, for clarity. For $0 < t < 2$ ms, ions are collected on the lower electrode, as indicated by an increasing voltage. For $t > 2$ ms, the collection of ions is no longer detectable, indicating that the afterglow has essentially ceased, so that the chamber has a lack of space charge, and it has a vacuum electric field. The bias for $t > 2$ ms was nearly steady during the time shown here; it diminished with an e-folding time 3 s, as explained in the text.

For $t > 2$ ms, after the ions were no longer detectable, there was a slow exponential decay in the electrode's bias. This decay occurred with an e-folding time of 3 s (which we attribute to the RC time for discharging C_{coupl} through a resistance of 60 MΩ that was mainly due to the 100X probe). For our purposes, the end of this time interval was t_{imp}, when the grains impacted on the lower electrode. (The value of t_{imp}, as tabulated in the supplementary material, was, for example, 41.67 ms for the run with a self-bias of −148 V.) Due to the long e-folding time of this decay, we can describe the electric potential on the lower electrode as a nearly steady bias during the time interval $2\text{ ms} < t < t_{\text{imp}}$, when our camera recorded the grains falling to the lower electrode. When we calculate the grain's charge, we will require the electric field in the time interval $2\text{ ms} < t < t_{\text{imp}}$, and for that purpose, when we will report $E_{t>2\text{ms}}$, we will report not a single value, but a range of values between two limits, corresponding to two times: $t = 2$ ms and the time t_{imp} when the grains impact the electrode.

2. Ion density estimation

The ion space charge during plasma operation, $t < 0$, can be estimated by analyzing the electrode voltage waveform.[70] For our experiment, in the waveform of Fig. 2, we use the overall change $\Delta V_{\text{electrode}}$ in the capacitor voltage during the time interval $0 < t < 2$ ms, when the electrode was still collecting ions. We assume that all the ions within the plasma volume collect on the lower electrode, since its negative voltage attracts ions much more than the grounded surface elsewhere in the chamber. Calculating the total charge of the ions within

the plasma volume as $C_{coupl}\,\Delta V_{electrode}$ and dividing by a plasma volume of 3.1 l yields a volume-averaged ion density,

$$n_i = C_{coupl}\Delta V_{electrode}/(3.1\,\mathrm{l}). \quad (8)$$

In this manner, for the run with a self-bias of −148 V, we obtain $\approx 1.8 \times 10^9$ cm^{-3} for the volume-averaged ion density, while the rf power was on. The corresponding total charge of the ions in the plasma volume was $\approx 5 \times 10^{12}$ e.

For the other runs, values for n_i are tabulated in the supplementary material. In general, as one would expect, the volume-averaged ion density trended upward with increasing rf power.

D. Photomultiplier tube measurements

The presence of energetic electrons is indicated by the visible glow, as detected by our photomultiplier tube. An electron energy >11 eV is required to excite a neutral Ar atom so that it subsequently emits a photon. Therefore, the glow serves primarily to indicate the presence of these energetic electrons.

The waveform for the glow was found to decay, after turning off the rf power, in two steps. The first step was rapid, with an e-folding time of 0.6 μs. This is the shortest timescale, for all the phenomena in our temporal afterglow, and we interpret this as the time for energetic electrons to cool, due to collisions with the gas. Later, starting about 2 μs, there was a slower decay of the glow intensity until it became almost undetectable at about 500 μs. This slower decay might be due to metastable neutral atoms. Waveforms are provided in the supplementary material.

E. Reignition test

In another test, which might be more sensitive than the PMT measurements of glow, we attempted to reignite the plasma after the rf power had been switched off for a specified time. In this test, we found that it was possible to reignite the plasma after waiting as long as 900 μs in the afterglow, but not longer. We interpret this result as indicating that at least some electrons were present until 900 μs; perhaps they were extremely few in number, and too cold to produce a detectable glow, but they were nevertheless present and available to start an avalanche of ionization when the rf field was applied once again.

F. Time scales in the afterglow

We can summarize the time sequence in our temporal afterglow, based on a combination of the measurements presented above and the theoretical literature.

Within a few microseconds of extinguishing the rf power, the energetic electrons are cooled by collisions with gas atoms. This rapid diminishment of energetic electrons is indicated by our glow measurement, decaying exponentially with a time constant of 0.6 μs.

By $t = 900$ μs, slow electrons have departed so completely that we are unable to reignite the plasma, if the rf power remains off. This experimentally obtained value of 900 μs is comparable to the theoretical time scale for transport of slow electrons to the walls, which we calculate as about 1.3 ms using the formula for τ_D^{∞} in Eq. (2) as in Ref. 25.

After the electrons have departed, ions continue to linger. They are so few in number that their space charge does not greatly affect the electric potential profile in the chamber, so that the electric potential profile is mostly like that of vacuum conditions. Ions continue to flow through the gas toward the negatively biased electrode, as detected by our measurement of the electrode bias.

Finally, for $t > 2$ ms the ions become undetectably sparse. With the space charge of ions now absent, the electric potential profile has completely relaxed to the vacuum condition.

G. Acceleration measurement

Our analysis centers on a measurement of the acceleration of grains, which we present here. As the grains fell, they were imaged at 600 frames/s using the side-view camera. An example video is provided in the supplementary material.

A composite image from one of our runs is shown in Fig. 3. Each grain appears as a streak, which has a vertical elongation due to the finite exposure time of 1.67 ms.

In analyzing each run, we tracked grains to obtain their height, velocity, and acceleration. The height of a grain was measured at the center of a streak; this measurement was done in each video frame, using the moment method[71] with ImageJ software.[81] The camera had an ample spatial resolution for this measurement. This analysis was done for all the grains visible in an image, which was always at least 30 grains. Their height was then averaged to yield a single value at the time the frame was recorded. Repeating this height measurement for each video frame, we obtained a time series of the vertical velocity, calculated as a finite difference, using the central differencing scheme. The velocity time series for one of our runs is plotted in Fig. 4, where the zero for the time axis takes into account our use of finite differences.

The downward acceleration was found to sustain a constant value, as seen in Fig. 4, where the velocity increases linearly with time.

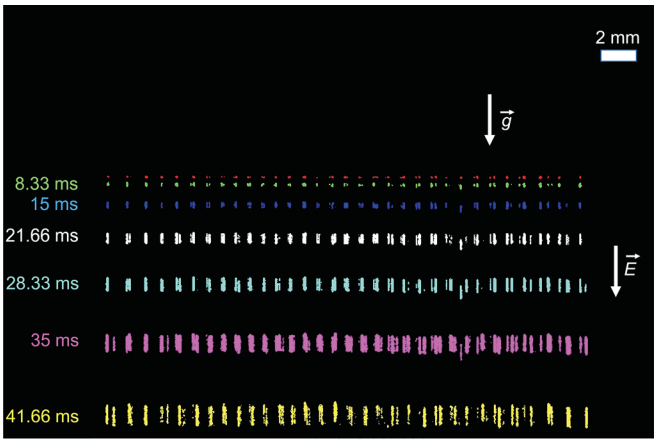

FIG. 3. Grains falling during the afterglow. This is a superposition of seven images, from the side-view camera, operated at 600 frames/s starting at $t = 0$, when the rf power was switched off. For this composite image, every fourth frame is shown. (The original video, including all frames, is provided in the supplementary material.) Two contributions to the grain's acceleration are both downward: gravity g and the vacuum electric field $E_{falling}$. Image analysis yields the position of the center of each streak corresponding to an individual grain. The run shown here had a self-bias of −148 V; grains started at $t = 0$ from a height of 14.34 mm, and they impacted the lower electrode at $t_{imp} = 41.67$ ms.

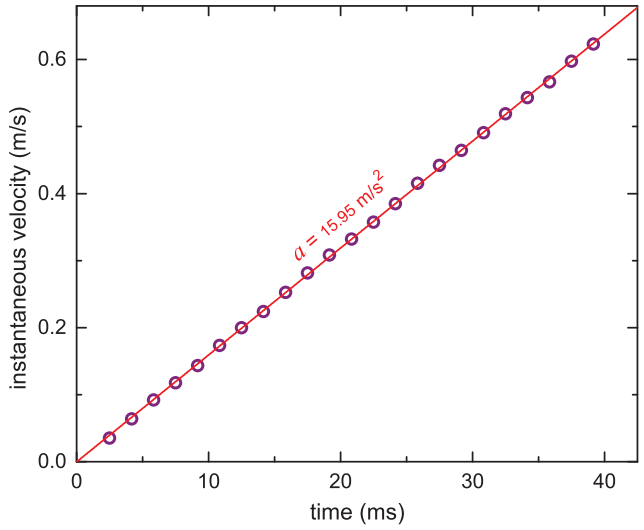

FIG. 4. Time series of instantaneous velocity, revealing the acceleration of the falling grains. These velocities were obtained as a finite difference, with an input of grain heights. (The velocity data points shown here were obtained entirely from positions at $t > 2$ ms, when the electric field had vacuum conditions.) The value of the acceleration is obtained from a linear fit, shown as a solid line. Results shown here are for the run with a dc self-bias of −148 V.

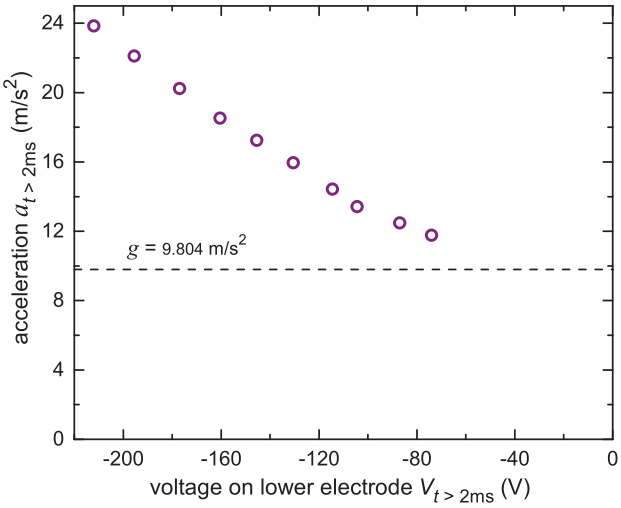

FIG. 5. Acceleration of grains. The value of the downward acceleration was obtained using a linear fit of velocity data, Fig. 4, for t > 2 ms. We find that the downward acceleration always exceeds that of gravity alone. The acceleration increases with an increasing potential on the lower electrode, indicating that the additional acceleration arises from an electrical force. For comparison, we indicate the local value of the acceleration of gravity, g.

We obtained the value of the acceleration by fitting the velocity time series to a line, with two free parameters. In this fit, we included the velocity data points obtained entirely from positions at $t > 2$ ms, when the electric field was for vacuum conditions.

Most significantly, the downward acceleration that we find is greater than that of gravity alone. Thus, there must be an additional downward force. Moreover, we found that the acceleration depends on the potential on the lower electrode, as shown in Fig. 5. This dependence suggests an electrical nature for an additional downward force.

V. ANALYSIS OF RESIDUAL CHARGE

A. Vacuum electric field

Our measurements of the acceleration of grains allows us to determine their residual charge. This analysis requires estimating the dc electric field. Fortunately, the electric field can be evaluated for vacuum conditions during the acceleration of the grains. The first acceleration data point is at 1.67 ms after the rf power was extinguished, and beyond that time, ions and electrons were diminished so greatly that their space charge was no longer a factor in determining the electric field.

Solving LaPlace's equation yielded the electric field values used in this analysis of the residual charge. The solution was done numerically, with cylindrically symmetric boundary conditions that closely mimic the physical chamber. As a check, we verified this numerical solution using an analytic solution, as described in the supplementary material.

We require the vertical component of the electric field, to evaluate the vertical acceleration. This vertical component had only a very weak radial variation, for the locations of our grains, so that with good accuracy we can analyze our acceleration data using the electric field evaluated at just a single radius of 1 cm. At that radius, the horizontal component, which was not required for our analysis, was 3.1% of the vertical component.

One of the boundary conditions, the lower electrode bias, depended on time. As discussed in Sec. IV C 1, this bias diminished slightly for $t > 2$ ms, due to the capacitor C_{coupl} discharging with an e-folding time of 3 s. To account for this weak time dependence, in our analysis of each run we used two values of the vertical component of the electric field. One value, $E_{charging}$, was for a position and time representative of the grains when they attained their final frozen charge. We evaluated $E_{charging}$ at a height of 14 mm, averaging over two times, $t = 0$ and $t = 2$ ms. The other value, $E_{falling}$, was for a height of 8 mm, which was representative of grains as they were observed to be falling.

B. Forces

Our approach for obtaining the charge from measurements of the acceleration is simply to use Newton's second law. This method is like that of Ticos *et al.*,[52] except that our grains fell during a temporal afterglow, not during steady plasma operation. We account for three forces acting on the grain: gravity, an electric force $Q_{res}E$ acting on the residual charge, and a gas friction force F_{fr} in the opposite direction,

$$F_{net} = m_d\, g + Q_{res}E - F_{fr} = m_d\, a. \quad (9)$$

No other forces were significant. In particular, thermophoretic forces were avoided by applying no heating or cooling to our chamber, and by using a low rf voltage. We verified that there was no detectable temperature increase on the lower electrode's surface. The ion drag force is absent because we use Eq. (9) only after 2 ms, when ions have already departed.

The gas friction force F_{fr}, unlike the other forces, varies strongly with time as the grains fall. Fortunately, F_{fr} can be neglected for our low gas pressure, as we explain here and in Subsection V C.

The magnitude of F_{fr} can be calculated using the Epstein formula,[72] which is applicable when the mean-free-path for gas–gas collisions is greater than the grain diameter,

$$F_{fr} = -\delta \frac{4}{3}\pi R^2 m_n v_{th} N v_d. \tag{10}$$

Here, m_n, N, and v_{th}, are the mass, number density, and thermal velocity of the neutral gas atoms, respectively, while v_d is the relative velocity between the grain and the gas. We use a coefficient $\delta \approx 1.35$ for our melamine-formaldehyde grains.[73] Evaluating Eq. (10), we find that F_{fr} attains a peak value that is rather small, at most a few percent of the gravitational force $m_d g$, at the end of the trajectory when the grain's velocity is greatest. Indeed, we determined that neglecting the gas friction force in Newton's second law, Eq. (9) will introduce a systematic error of at most 2% in our analysis of the residual charge, as explained in the supplementary material.

C. Residual charge

Solving Eq. (9) for the residual charge, and neglecting F_{fr}, we obtain

$$Q_{\text{res}} = \frac{m_d(a-g)}{E}. \tag{11}$$

If the electric field varies somewhat in position and time, as it does in our experiment, we must choose a particular value. For our experiment, we evaluate the electric field at a late time, under vacuum conditions, and at a position approximately midway through the fall of the grain. This value, as described in Sec. V A, is denoted E_{falling}, so that in our experiment we will evaluate the residual charge as

$$Q_{\text{res}} = \frac{m_d(a-g)}{E_{\text{falling}}}. \tag{12}$$

The corresponding potential on the grain's surface will be

$$V_{\text{float}} = \frac{Q_{\text{res}}}{4\pi\varepsilon_0 R}. \tag{13}$$

The inputs to Eqs. (12) and (13) are the grain's mass and radius m_d and R, along with a, g, and E_{falling}. The acceleration a was obtained from our image analysis. The acceleration of gravity is $g = 9.804$ m/s^2, based on standardized data for a location in the city of Cedar Rapids,[74] which is near our laboratory in Iowa City.

Our results for the residual charge are presented in Fig. 6. A striking feature of these results is the large value attained, for the positive charge. Our value of Q_{res} of the order of $+10^4$ e greatly exceed the positive charges that were reported for most of the earlier experiments.[32,43,47,60]

Another significant observation is that our measurements of the residual charge in Fig. 6 have little scatter, and our tests show good repeatability. We mention this because a wide distribution in residual charge was reported for a previous experiment.[60] To assess the consistency and repeatability of our results, we performed tests using three separate trials under the same conditions. As described in the supplementary material, in a grain-to-grain consistency test we found that acceleration of individual grains within a cloud varied by <1%. In a separate run-to-run repeatability test, the acceleration and residual charge were found to vary by only 2%, when using the same analysis methods as in the main experiment. These small variations give us confidence in using our experimental results to test our hypothesis.

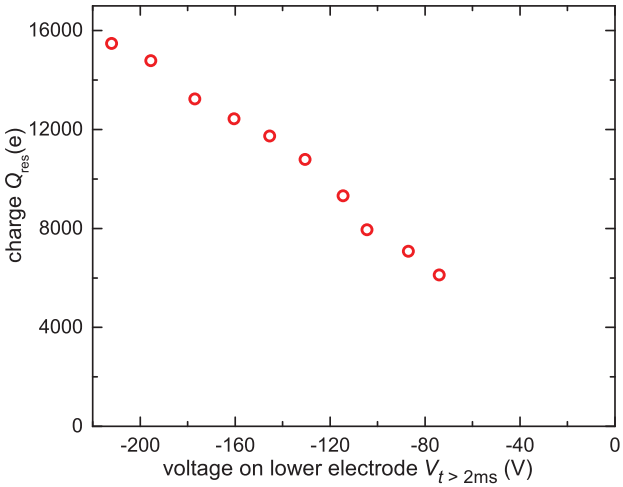

FIG. 6. Residual charge Q_{res}, on the grains, obtained from Eq. (12). Runs were performed at various rf amplitudes, leading to different dc voltages remaining on the lower electrode at $t > 2$ ms. Vertical error bars (due to the acceleration measurement) are not shown, as they would be smaller than the symbol size.

We can mention two sources of systematic error in our values for the residual charge in Fig. 6. These errors, which partially offset one another, arise from ignoring the two small effects: the frictional force F_{fr} and a loss of the grain's mass m_d. Neglecting the frictional force causes us to underestimate the residual charge by at most 2%, as explained in the supplementary material. Neglecting the mass loss, on the other hand, causes us to overestimate the residual charge, by up to 10%. The latter value is based on the experiments by others,[75,76] which showed that melamine-formaldehyde grains can lose up to 10% of their mass due to vacuum exposure. Since Q_{res} is proportional to m_d in Eq. (12), the value of Q_{res} we report in Fig. 6 could be too large, by as much as 10%.

VI. TESTING THE HYPOTHESIS FOR CHARGING WITH A DC ELECTRIC FIELD

Restating our hypothesis, after electrons have largely vanished, the residual charge is determined by the energy of the remaining ions as they drift in the presence of an externally applied electric field. As these drifting ions collect on a grain, it charges positively, but its surface potential eV_{float} cannot exceed a maximum value, which is the ion kinetic energy K_i. That kinetic energy is controlled by the reduced electric field, E/N. Thus, the maximum surface potential, and correspondingly the maximum residual charge of the grain, are determined by E/N.

To test this hypothesis, we will compare two quantities: the experimentally determined surface potential eV_{float}, and the kinetic energy K_i of mobility-limited ion motion as determined by the reduced electric field E/N. For this purpose, the value of the electric field of interest is E_{charging}, representative of the time and position when a grain attains its final frozen charge. Thus, we will calculate K_i using

$$K_i = \frac{1}{2} m_i \alpha^2 \left[1 + \beta \frac{E}{N}\right]^{-1} \left(\frac{E}{N}\right)^2, \tag{14}$$

with an input of the value of $E_{charging}/N$. Equation (14) is derived by combining Eq. (6) with the semi-empirical mobility-limited velocity, Eq. (5).

We should mention that our experiment was performed in a range $4000 < E/N < 11\,000$ Td that exceeded that of drift tube experiments, where E/N was at most 2000 Td. Thus, our use of Eq. (14) essentially involves an extrapolation of the known mobility data to a higher energy. We justify this extrapolation by noting that the ion mobility is determined mainly by charge–exchange collisions, which have a cross section that depends only weakly on the ion velocity.[64]

A. Present experiment

For a test using our experimental data, we start by converting the potential in the x axis of Fig. 6 to $E_{charging}/N$. This step, which uses our numerical solution of Laplace's equation, yields Fig. 7. We then use Eq. (13) to convert the y axis data in Fig. 7, from charge to the potential V_{float}, yielding Fig. 8(a).

As our chief result, we find that our experiment agrees with the theoretical curve. In Fig. 8(a), the bars for the experimental surface potential coincide with the curve for the ion kinetic energy. This agreement provides support for the hypothesis, for our experimental conditions.

This agreement also indicates that the residual charge reached its maximum possible value, in our experiment. As discussed in Sec. III A, if the charging time is too long, the grain will never reach its maximum possible value before the time it becomes frozen. The agreement between the curve for ion kinetic energy and the floating potential of the grains in Fig. 8(a) indicates that the grain charge did not become frozen prematurely, but had sufficient time to reach its maximum possible charge.

As one of our key points, we note in Fig. 8(a) that ion energies greater than 1 eV are easily attained in the afterglow, due to ions drifting in the presence of a dc electric field. Previous investigators assumed a much lower ion energy of about 0.025 eV, corresponding to room temperature, as we mentioned in Sec. III B. The much greater ion energy that prevailed in our experiment allows attaining a much greater positive charge than would be possible if the ions were not drifting.

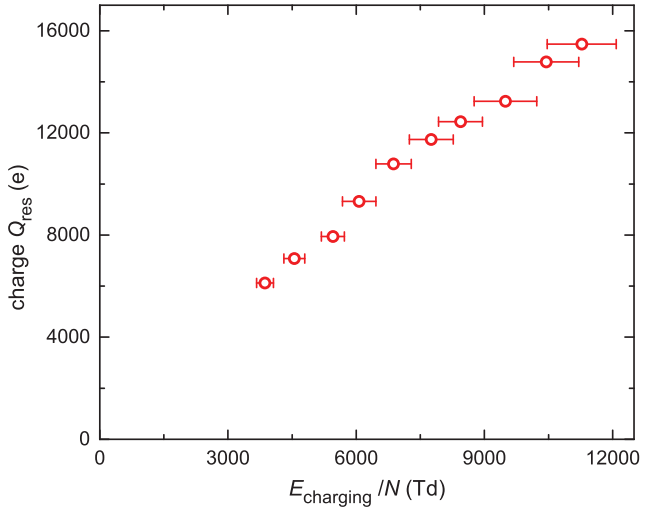

FIG. 7. Our same experimental data as in Fig. 6, replotted with E/N on the x axis. The magnitude of the electric field used here is $E_{charging}/N$ at a height of 14 mm, in the first few milliseconds when ions were present. The bars represent the full range of $E_{charging}/N$ as it varied slightly over time while ions were collected on the lower electrode; the data point indicates the midpoint of this range. The units on the x axis are Townsends, where $1\ \text{Td} = 10^{-17}\ \text{V cm}^2$.

B. Previous experiments

As a further test of our hypothesis, we present in Fig. 8(b) our analysis of the experiments of Wörner *et al.*[32] and Minderhout *et al.*[43] We calculated E/N, using the electric field and gas pressure reported by the original authors. We calculated the surface potential V_{float} using Eq. (13) with an input of values reported for the previous experiments for grain diameter and charge. Since the latter was reported as a range, we correspondingly report ranges of V_{float}, indicated as bars in Fig. 8(b); these are not error bars.

In Fig. 8(b), the experimental grain potential fell short of the theoretical ion kinetic energy. In other words, although grains charged to positive values, they did not reach the maximum possible positive potential, at which all ions are repelled from the grain. We can mention possible reasons for this shortfall, which were identified already by Wörner *et al.*[32]

One of the reasons for a shortfall in charging, as mentioned by Wörner *et al.*,[32] was physical and the other was related to instrumentation. The physical mechanism was a long charging time, in a temporal afterglow. If the charging time is too long (compared to the time for ions to be exhausted, either by drifting to the chamber walls or by collecting on the grains themselves in a three-dimensional cloud), the positive temporal variation in the grain's charge can cease prematurely. The instrumentation effect was the camera's limited spatial resolution, in the experiment of Wörner *et al.*, which could introduce errors in the measurements of the grain's position and cause the grain's displacement to be underestimated. That in turn could cause the charge to be underestimated, they suggested.

For the experiment of Minderhout *et al.*,[43] we propose that the presence of electrons was likely to limit the positive charging of the grains. This was because the authors used a spatial afterglow, i.e., the exhaust of a flowing plasma that was operated steadily; the plasma was not switched off to make a temporal afterglow, as in the present experiment or the experiment of Wörner *et al.* In a spatial afterglow, electrons are present to a much greater extent than in the late stages of a temporal afterglow. Thus, for the experiment of Minderhout *et al.*, we suggest that by steadily collecting electrons, grains were prevented from charging positively to a positive charge so large as to repel all ions.

VII. DUST AS A PROBE OF THE AFTERGLOW

Our results suggest a possible use of dust grains in plasmas, as a probe of afterglow plasmas. Traditional diagnostics of ions can be challenging in an afterglow plasma. In particular, the signal strength for laser-induced fluorescence[78,79] can be too weak in the absence of energetic electrons to excite the ions.

The advantage of using dust grains as a probe is that the signal that is detected is not from the ions themselves, but light scattered from the grains, and that light is just as bright in the afterglow as during plasma operation. A grain's acceleration can be measured easily using cameras, and this acceleration is an indication of a charge

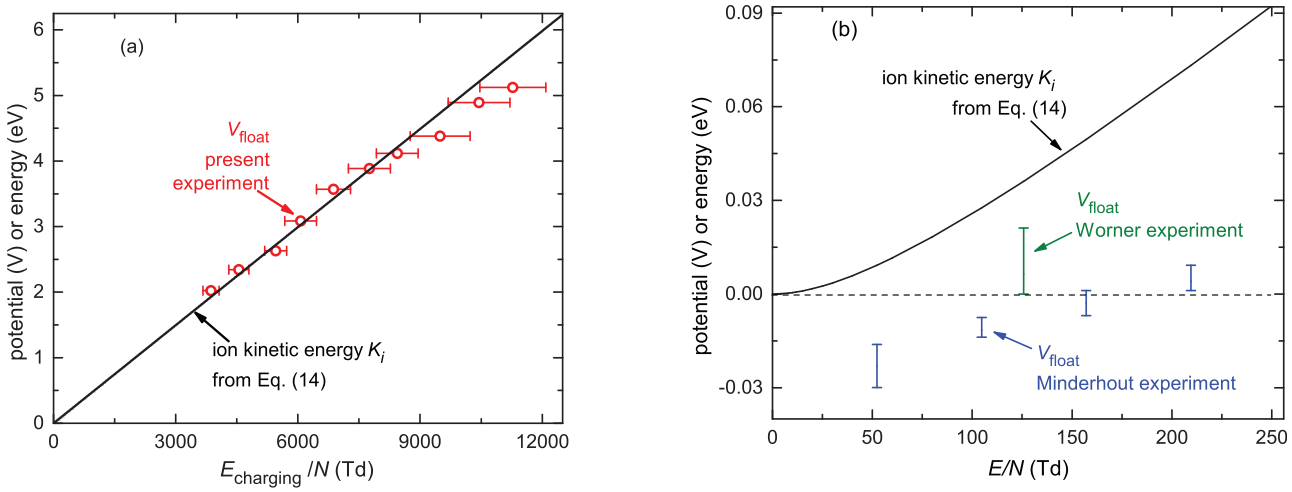

FIG. 8. Comparison of a grain's surface potential V_{float} obtained from Eq. (13) and the theoretical ion kinetic energy K_i obtained from Eq. (14). The latter assumes mobility-limited ion motion. (a) Data for our experiment, where the reduced electric field on the x axis, $E_{charging}/N$, is evaluated when ions were still present. The agreement of the two quantities in (a) is our most important result; it supports the hypothesis that the residual charge of our grains is explained by the collection of ions drifting in the dc electric field, for our experiment. (b) For previous experiments of Wörner *et al.*[32] and Minderhout *et al.*,[43] bars indicate the surface potential V_{float}, which we calculated using Eq. (13) with an input of the charge reported by the authors, without any adjustments. Bars correspond to the full range of the distribution of charges of grains reported by the authors. The theoretical curve for ion energy is the same as in (a). In these previous experiments, the potential fell short of our ion-kinetic-energy curve; this shortfall may be due to the effects that were absent in our experiment, as explained the text.

determined by the ion conditions at a particular time and height in the afterglow, as we have described in this paper. The floating surface potential can reach the energy of the ions, as it did in our experiment, and therefore, a measurement of the residual charge can be used as a diagnostic of ion energies.

We can suggest a variation of this diagnostic, to allow measuring ion conditions at not just one time in the afterglow, but various times. This would be enabled by using grains of various sizes, because of the inverse scaling of charging time and grain size in Eq. (2). The frozen-charge condition will occur later for a grain that is smaller. Thus, if an experimenter finds different surface potentials, for grains of different sizes, that would indicate the temporal development of the ion kinetic energy. Such an analysis could be done best if the experiment is performed under conditions where the maximum floating potential is attained, as in our experiment. Otherwise, if there are effects, such as a depletion of ions on the grains as in Ref. 32, this analysis could be hindered.

Another variation of the diagnostic would allow measurements of ion conditions at different heights. Rather than observing grains after they settle at a steady equilibrium height, as in our experiment, one could observe them earlier, as they fall from a dispenser, as in the experiment of Ref. 52. Differently from the experiment as in Ref. 52, the rf power could be switched off at the moment when the grains have fallen to the desired height, where one wishes to probe the ion conditions.

VIII. SUMMARY

We present an advance in the description of how grains can develop a positive charge in an afterglow plasma.

Previous work correctly identified, as a necessary condition for positive charging, a much greater abundance of ions than electrons.[25–27,29,32,43,47] Previous investigators also correctly emphasized the importance of the gradual diminishment of ion density, until the moment when the grain's charge becomes frozen, in a temporal afterglow.[25–27,29,32] A dc electric field served a significant role in previous afterglow experiments to allow the detection of a grain's charge.[25,32,43,47,60] Another role of the electric field that has been reported, specifically for a spatial afterglow, is a modification of the density of uncompensated ions, which can affect the grain's charging.[43]

In the present paper, we emphasized yet another role for the electric field: maintaining an ion kinetic energy that exceeds the room-temperature thermal energy. We hypothesized that this greater ion energy, due to a dc electric field, will in turn lead to the collection of a greater positive charge on a grain, at a time after the electrons have largely departed. The maximum value that this residual charge can attain can be calculated for a given value of the reduced electric field E/N. This maximum value assumes ion motion that is mobility limited, which is valid if the ion-neutral mean-free-path is much shorter than the chamber size.

We tested this hypothesis using data from a temporal afterglow experiment. We prepared a layer of dust grains, levitated above a negatively biased lower electrode. We then switched off the rf power that sustained the plasma, while a negative bias remained on the electrode, creating a vertical electric field that could accelerate a grain. We imaged the grains, as they fell, with adequate spatial and temporal resolution to obtain precise and repeatable values for their acceleration. These images, which were recorded after ions were generally absent, allowed us to measure the acceleration of grains. A simple equation of

motion, along with a calculated vacuum electric field, then yielded the residual charge of the dust grains, during their fall.

The residual charge Q_{res} was found to have a large positive value of thousands of elementary charges. In our experiment, E/N had a large value due to a low gas pressure, so that we could attain a larger charge than in previous temporal-afterglow experiments.[32,60]

Using the value of Q_{res}, we calculated the residual surface potential V_{float}, which had a typical value of a few volts in our experiment. The value of V_{float} allows the testing of charging models for the afterglow, and in particular, it allows testing our hypothesis.

Our experiment provides quantitative support for the hypothesis. The surface potential of our dust grains was found to agree well with the ion energies predicted for mobility-limited ion motion, and this agreement holds over the entire range of electric field that we tested.

We suggest two practical applications of this mechanism of applying a dc electric field to adjust the ion drift velocity in the afterglow. First, applying an electric field is a means for controlling a grain's residual charge. There is a straightforward relationship between this electric field and the residual charge on the dust grains, under the conditions of our experiment. Second, applying a field and measuring the grain's acceleration may allow the use of grains as probes, for diagnosing the conditions within an afterglow plasma.

SUPPLEMENTARY MATERIAL

See the supplementary material for experimental data including waveforms and a video of grains falling, details of apparatus, table of experimental runs, estimation of error due to gas friction, repeatability test, vacuum electric field calculation, and simulation results describing the plasma conditions before the rf power was extinguished.

ACKNOWLEDGMENTS

We thank S. Ruhunusiri and A. Kananovich for designing and building the chamber and optical system, and for providing diagrams incorporated in our Fig. 1 and our supplementary material. We thank U. Kortshagen and E. Thimsen for helpful discussions. This work was supported by the Army Research Office under MURI Grant No. W911NF-18-1-0240, U.S. Department of Energy Grant No. DE-SC0014566, and NASA JPL Subcontract No. 1663801.

AUTHOR DECLARATIONS

Conflict of Interest

The authors have no conflicts to disclose.

DATA AVAILABILITY

The data that support the findings of this study are available within the article and its supplementary material.

REFERENCES

[1]P. K. Shukla and A. A. Mamun, *Introduction to Dusty Plasma Physics*, Series in Plasma Physics (Institute of Physics Publishing, 2001).
[2]P. M. Bellan, *Fundamentals of Plasma Physics* (Cambridge University Press, 2008), Chap. 17, pp. 483–506.
[3]A. Piel, "Chapter 10: Dusty plasmas," in *Plasma Physics: An Introduction to Laboratory, Space, and Fusion Plasmas* (Springer, Berlin, 2010), pp. 259–321.
[4]A. Melzer, *Physics of Dusty Plasmas, Lecture Notes in Physics* (Springer International Publishing, Cham, 2019), Vol. 962.
[5]V. E. Fortov, A. G. Khrapak, S. A. Khrapak, V. I. Molotkov, and O. F. Petrov, "Dusty plasmas," Phys.-Usp. **47**, 447–492 (2004).
[6]V. N. Tsytovich, G. E. Morfill, S. V. Vladimirov, and H. M. Thomas, "Elementary processes in complex plasmas," in *Elementary Physics of Complex Plasmas* (Springer Berlin Heidelberg, Berlin, Heidelberg, 2008), pp. 67–140.
[7]A. Melzer and J. Goree, "Chapter 6: Fundamentals of dusty plasmas," in *Low Temperature Plasmas: Fundamentals, Technologies and Techniques*, 2nd ed., edited by R. Hippler, H. Kersten, M. Schmidt, and K. H. Schoenbach (Wiley-VCH, Weinheim, 2008), p. 129.
[8]M. Bonitz, C. Henning, and D. Block, "Complex plasmas: A laboratory for strong correlations," Rep. Prog. Phys. **73**, 066501 (2010).
[9]C. K. Goertz, "Dusty plasmas in the solar system," Rev. Geophys. **27**, 271–292, https://doi.org/10.1029/RG027i002p00271 (1989).
[10]E. C. Whipple, "Potentials of surfaces in space," Rep. Prog. Phys. **44**, 1197–1250 (1981).
[11]J. E. Colwell, S. R. Robertson, M. Horányi, X. Wang, A. Poppe, and P. Wheeler, "Lunar dust levitation," J. Aerosp. Eng. **22**, 2–9 (2009).
[12]X. Wang, M. Horányi, and S. Robertson, "Experiments on dust transport in plasma to investigate the origin of the lunar horizon glow," J. Geophys. Res. **114**, A05103, https://doi.org/10.1029/2008JA013983 (2009).
[13]R. D. Smirnov, A. Y. Pigarov, M. Rosenberg, S. I. Krasheninnikov, and D. A. Mendis, "Modelling of dynamics and transport of carbon dust particles in tokamaks," Plasma Phys. Controlled Fusion **49**, 347–371 (2007).
[14]H. Thomas, G. E. Morfill, V. Demmel, J. Goree, B. Feuerbacher, and D. Möhlmann, "Plasma crystal: Coulomb crystallization in a dusty plasma," Phys. Rev. Lett. **73**, 652–655 (1994).
[15]T. Trottenberg, A. Melzer, and A. Piel, "Measurement of the electric charge on particulates forming coulomb crystals in the sheath of a radiofrequency plasma," Plasma Sources Sci. Technol. **4**, 450–458 (1995).
[16]E. Thomas and M. Watson, "Charging of silica particles in an argon dusty plasma," Phys. Plasmas **7**, 3194–3197 (2000).
[17]V. Nosenko, J. Goree, Z. W. Ma, D. H. E. Dubin, and A. Piel, "Compressional and shear wakes in a two-dimensional dusty plasma crystal," Phys. Rev. E **68**, 056409 (2003).
[18]S. Ratynskaia, S. Khrapak, A. Zobnin, M. H. Thoma, M. Kretschmer, A. Usachev, V. Yaroshenko, R. A. Quinn, G. E. Morfill, O. Petrov, and V. Fortov, "Experimental determination of dust-particle charge in a discharge plasma at elevated pressures," Phys. Rev. Lett. **93**, 085001 (2004).
[19]S. A. Khrapak, S. V. Ratynskaia, A. V. Zobnin, A. D. Usachev, V. V. Yaroshenko, M. H. Thoma, M. Kretschmer, H. Höfner, G. E. Morfill, O. F. Petrov, and V. E. Fortov, "Particle charge in the bulk of gas discharges," Phys. Rev. E **72**, 016406 (2005).
[20]X. Wang, J. Colwell, M. Horanyi, and S. Robertson, "Charge of dust on surfaces in plasma," IEEE Trans. Plasma Sci. **35**, 271–279 (2007).
[21]A. Douglass, V. Land, L. Matthews, and T. Hyde, "Dust particle charge in plasma with ion flow and electron depletion near plasma boundaries," Phys. Plasmas **18**, 083706 (2011).
[22]M. Choudhary, S. Mukherjee, and P. Bandyopadhyay, "Transport and trapping of dust particles in a potential well created by inductively coupled diffused plasmas," Rev. Sci. Instrum. **87**, 053505 (2016).
[23]E. Thomas, U. Konopka, R. L. Merlino, and M. Rosenberg, "Initial measurements of two- and three-dimensional ordering, waves, and plasma filamentation in the magnetized dusty plasma experiment," Phys. Plasmas **23**, 055701 (2016).
[24]M. Choudhary, S. Mukherjee, and P. Bandyopadhyay, "Experimental observation of self excited co-rotating multiple vortices in a dusty plasma with inhomogeneous plasma background," Phys. Plasmas **24**, 033703 (2017).
[25]A. V. Ivlev, M. Kretschmer, M. Zuzic, G. E. Morfill, H. Rothermel, H. M. Thomas, V. E. Fortov, V. I. Molotkov, A. P. Nefedov, A. M. Lipaev, O. F. Petrov, Y. M. Baturin, A. I. Ivanov, and J. Goree, "Decharging of complex plasmas: First kinetic observations," Phys. Rev. Lett. **90**, 055003 (2003).
[26]L. Couëdel, M. Mikikian, L. Boufendi, and A. A. Samarian, "Residual dust charges in discharge afterglow," Phys. Rev. E **74**, 026403 (2006).
[27]L. Couëdel, A. A. Samarian, M. Mikikian, and L. Boufendi, "Influence of the ambipolar-to-free diffusion transition on dust particle charge in a complex plasma afterglow," Phys. Plasmas **15**, 063705 (2008).
[28]L. Couëdel, A. Samarian, M. Mikikian, and L. Boufendi, "Dust density effect on complex plasma decay," Phys. Lett. A **372**, 5336–5339 (2008).

[29]L. Couëdel, A. Mezeghrane, A. Samarian, M. Mikikian, Y. Tessier, M. Cavarroc, and L. Boufendi, "Complex plasma afterglow," Contrib. Plasma Phys. **49**, 235–259 (2009).
[30]I. V. Schweigert and A. L. Alexandrov, "Effect of nanoparticles on an rf discharge afterglow," J. Phys. D **45**, 325201 (2012).
[31]V. Saxena, K. Avinash, and A. Sen, "Dust cluster explosion," Phys. Plasmas **19**, 093706 (2012).
[32]L. Wörner, A. V. Ivlev, L. Couëdel, P. Huber, M. Schwabe, T. Hagl, M. Mikikian, L. Boufendi, A. Skvortsov, A. M. Lipaev, V. I. Molotkov, O. F. Petrov, V. E. Fortov, H. M. Thomas, and G. E. Morfill, "The effect of a direct current field on the microparticle charge in the plasma afterglow," Phys. Plasmas **20**, 123702 (2013).
[33]I. B. Denysenko, I. Stefanović, B. Sikimić, J. Winter, and N. A. Azarenkov, "Discharging of dust particles in the afterglow of plasma with large dust density," Phys. Rev. E **88**, 023104 (2013).
[34]I. B. Denysenko, I. Stefanovic, N. A. Azarenkov, and G. P. Burmaka, "Effect of secondary emission on the argon plasma afterglow with large dust density," Phys. Plasmas **22**, 023702 (2015).
[35]I. B. Denysenko, H. Kersten, and N. A. Azarenkov, "Electron energy distribution function, effective electron temperature, and dust charge in the temporal afterglow of a plasma," Phys. Plasmas **23**, 053704 (2016).
[36]I. B. Denysenko, N. A. Azarenkov, K. Ostrikov, and M. Y. Yu, "Electron energy probability function in the temporal afterglow of a dusty plasma," Phys. Plasmas **25**, 013703 (2018).
[37]A. Piel and J. A. Goree, "Collisional and collisionless expansion of Yukawa balls," Phys. Rev. E **88**, 063103 (2013).
[38]R. L. Merlino, J. K. Meyer, K. Avinash, and A. Sen, "Coulomb fission of a dusty plasma," Phys. Plasmas **23**, 064506 (2016).
[39]J. K. Meyer and R. L. Merlino, "Evolution of dust clouds in afterglow plasmas," IEEE Trans. Plasma Sci. **44**, 473–478 (2016).
[40]R. L. Merlino, J. K. Meyer, A. Barkan, K. Avinash, and A. Sen, "Coulomb explosion and fission of charged dust clusters," AIP Conf. Proc. **1925**, 020021 (2018).
[41]M. Chaudhuri, L. Couëdel, E. Thomas, P. Huber, A. M. Lipaev, H. M. Thomas, and M. Schwabe, "Spontaneous dust pulse formation in the afterglow of complex plasmas under microgravity conditions," arXiv:2103.09607 (2021).
[42]B. van Minderhout, T. Peijnenburg, P. Blom, J. M. Vogels, G. M. W. Kroesen, and J. Beckers, "The charge of micro-particles in a low pressure spatial plasma afterglow," J. Phys. D **52**, 32LT03 (2019).
[43]B. van Minderhout, J. C. A. van Huijstee, B. Platier, T. Peijnenburg, P. Blom, G. M. W. Kroesen, and J. Beckers, "Charge control of microparticles in a shielded plasma afterglow," Plasma Sources Sci. Technol. **29**, 065005 (2020).
[44]B. van Minderhout, J. C. A. van Huijstee, R. M. H. Rompelberg, A. Post, A. T. A. Peijnenburg, P. Blom, and J. Beckers, "Charge of clustered microparticles measured in spatial plasma afterglows follows the smallest enclosing sphere model," Nat. Commun. **12**, 4692 (2021).
[45]G. Sharma, N. Abuyazid, S. Dhawan, S. Kshirsagar, R. M. Sankaran, and P. Biswas, "Characterization of particle charging in low-temperature, atmospheric-pressure, flow-through plasmas," J. Phys. D **53**, 245204 (2020).
[46]V. Suresh, L. Li, J. R. G. Felipe, and R. Gopalakrishnan, "Modeling nanoparticle charge distribution in the afterglow of non-thermal plasmas and comparison with measurements," J. Phys. D **54**, 275205 (2021).
[47]B. van Minderhout, J. C. A. van Huijstee, A. T. A. Peijnenburg, P. Blom, G. M. W. Kroesen, and J. Beckers, "Charge neutralisation of microparticles by pulsing a low-pressure shielded spatial plasma afterglow," Plasma Sources Sci. Technol. **30**, 045016 (2021).
[48]E. Husmann, E. Thimsen, and X. Chen, "Particle charge distributions in the effluent of a flow-through atmospheric pressure low temperature plasma," Plasma Sources Sci. Technol. **30**, 075030 (2021).
[49]N. J. Kramer, R. J. Anthony, M. Mamunuru, E. S. Aydil, and U. R. Kortshagen, "Plasma-induced crystallization of silicon nanoparticles," J. Phys. D **47**, 075202 (2014).
[50]X. Chen, T. Seto, U. R. Kortshagen, and C. J. Hogan, "Size and structural characterization of si nanocrystal aggregates from a low pressure nonthermal plasma reactor," Powder Technol. **373**, 164–173 (2020).
[51]C. A. Beaudette, H. P. Andaraarachchi, C.-C. Wu, and U. R. Kortshagen, "Inductively coupled nonthermal plasma synthesis of aluminum nanoparticles," Nanotechnology **32**, 395601 (2021).
[52]C. M. Ticos, A. Dyson, and P. W. Smith, "The charge on falling dust particles in a RF plasma with DC negative bias," Plasma Sources Sci. Technol. **13**, 395–402 (2004).
[53]K. S. Ashrafi, R. Yousefi, M. Chen, L. S. Matthews, and T. W. Hyde, "Dust as probes: Determining confinement and interaction forces," Phys. Rev. E **102**, 043210 (2020).
[54]G. A. Hebner, M. E. Riley, and K. E. Greenberg, "Analysis of the particle interactions in a two-dimensional-plasma dust crystal and the use of dust as a probe of the time-averaged presheath electric field," Phys. Rev. E **66**, 046407 (2002).
[55]J. Beckers, T. Ockenga, M. Wolter, W. W. Stoffels, J. van Dijk, H. Kersten, and G. M. W. Kroesen, "Microparticles in a collisional rf plasma sheath under hypergravity conditions as probes for the electric field strength and the particle charge," Phys. Rev. Lett. **106**, 115002 (2011).
[56]H. Maurer, V. Schneider, M. Wolter, R. Basner, T. Trottenberg, and H. Kersten, "Microparticles as plasma diagnostic tools," Contrib. Plasma Phys. **51**, 218–227 (2011).
[57]P. Hartmann, A. Z. Kovács, J. C. Reyes, L. S. Matthews, and T. W. Hyde, "Dust as probe for horizontal field distribution in low pressure gas discharges," Plasma Sources Sci. Technol. **23**, 045008 (2014).
[58]A. Douglass, V. Land, K. Qiao, L. Matthews, and T. Hyde, "Using dust as probes to determine sheath extent and structure," J. Plasma Phys. **82**, 615820402 (2016).
[59]T. Antonova, S. A. Khrapak, M. Y. Pustylnik, M. Rubin-Zuzic, H. M. Thomas, A. M. Lipaev, A. D. Usachev, V. I. Molotkov, and M. H. Thoma, "Particle charge in PK-4 dc discharge from ground-based and microgravity experiments," Phys. Plasmas **26**, 113703 (2019).
[60]V. Schneider, "Optisch gefangene Mikropartikel als Sonden in einem Hochfrequenz-Niederdruckplasma," Ph.D. thesis (University of Kiel, 2020).
[61]C. Cui and J. Goree, "Fluctuations of the charge on a dust grain in a plasma," IEEE Trans. Plasma Sci. **22**, 151–158 (1994).
[62]J. Goree, "Charging of particles in a plasma," Plasma Sources Sci. Technol. **3**, 400–406 (1994).
[63]S. Robertson and Z. Sternovsky, "Monte Carlo model of ion mobility and diffusion for low and high electric fields," Phys. Rev. E **67**, 046405 (2003).
[64]B. M. Smirnov, *Theory of Gas Discharge Plasma* (Springer, Cham, 2015).
[65]L. S. Frost, "Effect of variable ionic mobility on ambipolar diffusion," Phys. Rev. **105**, 354–356 (1957).
[66]S. A. Khrapak and A. G. Khrapak, "Modified Frost formula for the mobilities of positive ions in their parent gases," AIP Adv. **9**, 095008 (2019).
[67]H. Ellis, R. Pai, E. McDaniel, E. Mason, and L. Viehland, "Transport properties of gaseous ions over a wide energy range," At. Data Nucl. Data Tables **17**, 177–210 (1976).
[68]W. D. S. Ruhunusiri, "Investigation of collective phenomena in dusty plasmas," Ph.D. thesis (The University of Iowa, 2014).
[69]A. Kananovich and J. Goree, "Experimental determination of shock speed versus exciter speed in a two-dimensional dusty plasma," Phys. Rev. E **101**, 043211 (2020).
[70]B. Sikimić, I. Stefanović, I. B. Denysenko, and J. Winter, "A non-invasive technique to determine ion fluxes and ion densities in reactive and non-reactive pulsed plasmas," Plasma Sources Sci. Technol. **22**, 045009 (2013).
[71]Y. Feng, J. Goree, and B. Liu, "Accurate particle position measurement from images," Rev. Sci. Instrum. **78**, 053704 (2007).
[72]P. S. Epstein, "On the resistance experienced by spheres in their motion through gases," Phys. Rev. **23**, 710–733 (1924).
[73]B. Liu, J. Goree, V. Nosenko, and L. Boufendi, "Radiation pressure and gas drag forces on a melamine-formaldehyde microsphere in a dusty plasma," Phys. Plasmas **10**, 9–20 (2003).
[74]N. K. Pavlis, S. A. Holmes, S. C. Kenyon, and J. K. Factor, "The development and evaluation of the Earth gravitational model 2008 (EGM2008)," J. Geophys. Res. **117**, B04406, https://doi.org/10.1029/2011JB008916 (2012).
[75]J. Pavlu, A. Velyhan, I. Richterova, Z. Nemecek, J. Safrankova, I. Cermak, and P. Zilavy, "Mass-loss rate for MF resin microspheres," IEEE Trans. Plasma Sci. **32**, 704–708 (2004).

[76]J. Carstensen, H. Jung, F. Greiner, and A. Piel, "Mass changes of microparticles in a plasma observed by a phase-resolved resonance method," Phys. Plasmas **18**, 033701 (2011).
[77]C. Qu, S. J. Lanham, S. C. Shannon, S. K. Nam, and M. J. Kushner, "Power matching to pulsed inductively coupled plasmas," J. Appl. Phys. **127**, 133302 (2020).
[78]M. J. Goeckner, J. Goree, and T. E. Sheridan, "Saturation broadening of laser-induced fluorescence from plasma ions," Rev. Sci. Instrum. **64**, 996–1000 (1993).
[79]F. Chu and F. Skiff, "A Lagrangian model for laser-induced fluorescence and its application to measurements of plasma ion temperature and electrostatic waves," Phys. Plasmas **25**, 013506 (2018).
[80]See http://www.microparticles.de/ for "Purchased from Microparticles GmbH (Volmerstr. 9A, D-12489 Berlin, Germany."
[81]W. S. Rasband, see https://imagej.nih.gov/ij for "Computer Code ImageJ, U. S. National Institutes of Health, Bethesda, Maryland, USA, 1997–2018."